

1 Type of the Paper (Article)

2 Metal-free modified boron nitride for enhanced CO₂ 3 capture

4 Fereshteh Hojatisaeidi¹, Mauro Mureddu², Federica Dessì², Geraldine Durand^{1,3} and Basudeb
5 Saha¹, *

6 ¹ School of Engineering, London South Bank University, 103 Borough Road, London SE1 0AA, United
7 Kingdom

8 ² Sotacarbo S.p.A. Grande Miniera di Serbariu, 09013 Carbonia (CA), Italy

9 ³ The Welding Institute, Granta Park, Great Abington, Cambridge, CB21 6AL, United Kingdom

10 * Corresponding Author: School of Engineering, London South Bank University, 103 Borough Road, London
11 SE1 0AA. Tel.: +44 (0)20 7815 7190; Fax: +44 (0)20 7815 7699. E-mail address: b.saha@lsbu.ac.uk (B. Saha).

12 **Abstract:** Porous boron nitride is a new class of solid adsorbent with applications in CO₂ capture. In
13 order to further enhance the adsorption capacities of materials, new strategies such as porosity
14 tuning, element doping and surface modification have been taken into account. In this work, metal-
15 free modification of porous boron nitride (BN) has been prepared by a structure directing agent *via*
16 simple heat treatment under N₂ flow. We have demonstrated that textural properties of BN play a
17 pivotal role in CO₂ adsorption behavior. Therefore, addition of a triblock copolymer surfactant
18 (P123) has been adopted to improve the pore ordering and textural properties of porous BN and its
19 influence on the morphological and structural properties of pristine BN has been characterised. The
20 obtained BN-P123 exhibits a high surface area of 476 m²/g, a large pore volume of 0.83 cm³/g with
21 an abundance of micropores. More importantly, after modification with P123 copolymer, the
22 capacity of pure CO₂ on porous BN has improved by about 34.5% compared to pristine BN (2.69
23 mmol/g for BN-P123 *vs.* 2 mmol/g for pristine BN under ambient condition). The unique
24 characteristics of boron nitride opens up new routes for designing porous BN, which could be
25 employed for optimizing CO₂ adsorption.

26 **Keywords:** Porous boron nitride; metal-free modification; structure directing agent; CO₂ capture.
27

28 1. Introduction

29 Over the last decades, climate change has become a global challenge for countries across the
30 world [1]. Carbon capture and storage (CCS) is expected to play a substantial role in meeting the
31 global warming targets set by the Inter-governmental Panel on Climate Change (IPCC) [2]. It is a
32 promising option to maintain fossil fuels as a global central energy contributor and is expected to
33 progress in lab scale, pilot scale, demonstration scale and commercial scale [3]. Chemical absorption
34 technology, which has been used to remove CO₂ from natural gas, is reached to the commercial phase
35 of development and several pilot-scale projects have been conducted since decades ago [4,5]. To date,
36 the capture technologies that have been demonstrated in pilot plant scale or higher are classified as
37 (i) post-combustion, (ii) pre-combustion, and (iii) oxy-fuel combustion [6]. Among the current
38 available technologies, CO₂ capture from post-combustion emission gases is the most common
39 technology in power plants and industries. Effective methods to separate, capture, store and convert
40 CO₂ have attracted increasing attention [7]. The current technology for CO₂ capture is based on
41 absorption in aqueous organic amines [8]. However, the intensive energy consumption, equipment
42 corrosion and toxicity, make exploration of new materials for CO₂ capture highly demanding [9].

43 Solid adsorption is an alternative process to solvent-based chemisorption, which can be applied
44 for a wide range of temperature and pressure conditions. Also, it can be designed for both post-
45 combustion and pre-combustion applications. One of the challenges in this area relates to the
46 manufacturing of new adsorbents that enables enhancing good diffusion kinetics and providing

47 improved performance [10]. In this regards, porous materials with high porosity, chemical and
48 thermal stability are promising solid adsorbents for capturing CO₂ [11,12]. Among various kinds of
49 porous materials, such as zeolites [13,14], porous polymers [15], metal-organic framework [16,17],
50 activated carbons [18], porous BN has become one of the new classes of CO₂ adsorbents. Due to
51 intrinsic properties of boron nitride such as high thermal and oxidation stability, large surface area
52 and polarity, porous boron nitride is a desired alternative for CO₂ capture [19,20]. However,
53 according to theoretical and experimental works, the interaction between pristine BN and CO₂ is very
54 weak due to electron deficient nature of boron atoms and the Lewis acidic nature of CO₂ [21,22,23].
55 To overcome such disadvantages, some strategies in view of tuning the structure, pore size and
56 charge state of the BN have been studied. Nag et al. [24] made a few-layered BN by controlled
57 chemical synthesis. Similarly, the effects of different proportions of urea on the number of BN layers
58 indicate that the sample with the lowest layer thickness shows a high CO₂ uptake. Xiao et al. [25]
59 reported a few layered porous boron nitride nanosheets (BNNs) by using magnesium diboride
60 (MgB₂) as a dynamic template. However, the CO₂ uptake of their work was relatively low (0.45
61 mmol/g), while it demonstrated excellent selectivity of CO₂ over N₂. Yang et al. [26] developed a three
62 dimensional (3D) functionalized porous BN with flower-like morphology and high specific surface
63 area ~1114 m²/g, and it shows 1.69 mmol/g CO₂ capture capacity at 1 bar and 273 K. It is also
64 interesting to note that in most studies, element doping, and surface functionalization of boron nitride
65 is critical to increase the CO₂ adsorption capacity. For instance, Chen et al. [27] produced ultrahigh
66 microporous volume of boron carbon nitride (BCN) by doping carbon into hexagonal structure of
67 BN. The performance of BCN material displays increased relative to pure BN for CO₂ uptake and
68 reached up to 3.91 mmol/g at 298 K and ambient pressure. In addition, Huang et al. [28] enriched the
69 interaction between electron-deficient boron atoms in BN and CO₂ molecules by aminopolymer-
70 functionalized BN nanosheets. Therefore, porous structure and surface chemistry features of BN-
71 based materials play crucial roles in CO₂ adsorption performance and it remains a challenge to control
72 the parameters of boron nitride porosity and develop novel structures with high capacitive
73 performance for carbon capture.

74 In this work, with the aim of achieving high CO₂ adsorption capacity of porous BN through
75 tuning the porosity, BN structure has been modified in the presence of P123 as a structure directing
76 agent. The synthesized BN-P123 possesses high specific surface area and pore volume compared to
77 pristine BN, which results in an enhanced CO₂ adsorption capacity.

78 2. Materials and Methods

79 Metal-free modified BN was synthesized on a two-step method of solvent evaporation and high
80 thermal decomposition [29]. Boric acid (ACS reagent, Sigma-Aldrich), urea (for synthesis, Sigma-
81 Aldrich) and Pluronic P123 triblock copolymers (M_n ~5800, Sigma-Aldrich) based on poly(ethylene
82 glycol)-poly(propylene glycol)-poly(ethylene glycol) were used as raw materials. In detail, boric acid
83 and urea with molar ratio 1:30 were added into 50 ml deionized water. Then 0.5 g P123 was
84 introduced into the mixture solution and heated up at 338 K under vigorous stirring. A white
85 precipitate was obtained after complete evaporation of water at that temperature. Afterwards, the
86 precursor was dried into the oven for 24 hours and annealed at 1173 K under N₂ gas (the flow rate is
87 150 ml/min) for 3 hours. Finally, modified porous BN was collected and marked as BN-P123. For
88 comparison, pristine BN was also prepared following the same procedure without adding any
89 surfactant.

90 The morphology of samples was collected scanning electron microscope (SEM, PEMTRON PS-
91 230) in secondary electron mode (SE detector) at 10 kV. The microscope was equipped with an
92 energy-dispersive X-ray (EDX, OXFORD X-act) with energy resolution at 5.9 keV for the local
93 elemental analysis. The samples were ground, deposited on carbon tape, and coated (BIO-RAD
94 sputter coater) with gold to reduce charging in the microscope.

95 X-ray diffraction (XRD) was performed to evaluate the structural properties using an X-ray
96 diffractometer (Bruker D8 Advance) in reflection mode. The diffraction patterns run at an anode
97 voltage of 40 kV and an emission current of 40 mA using monochromatic Cu K α radiation (λ = 1.541
98 78 Å). The intermolecular bonding and chemical properties of the materials were characterized by
99 Fourier-transform infrared (FTIR) spectroscopy. The spectra were recorded on a Nicolet Avatar 370

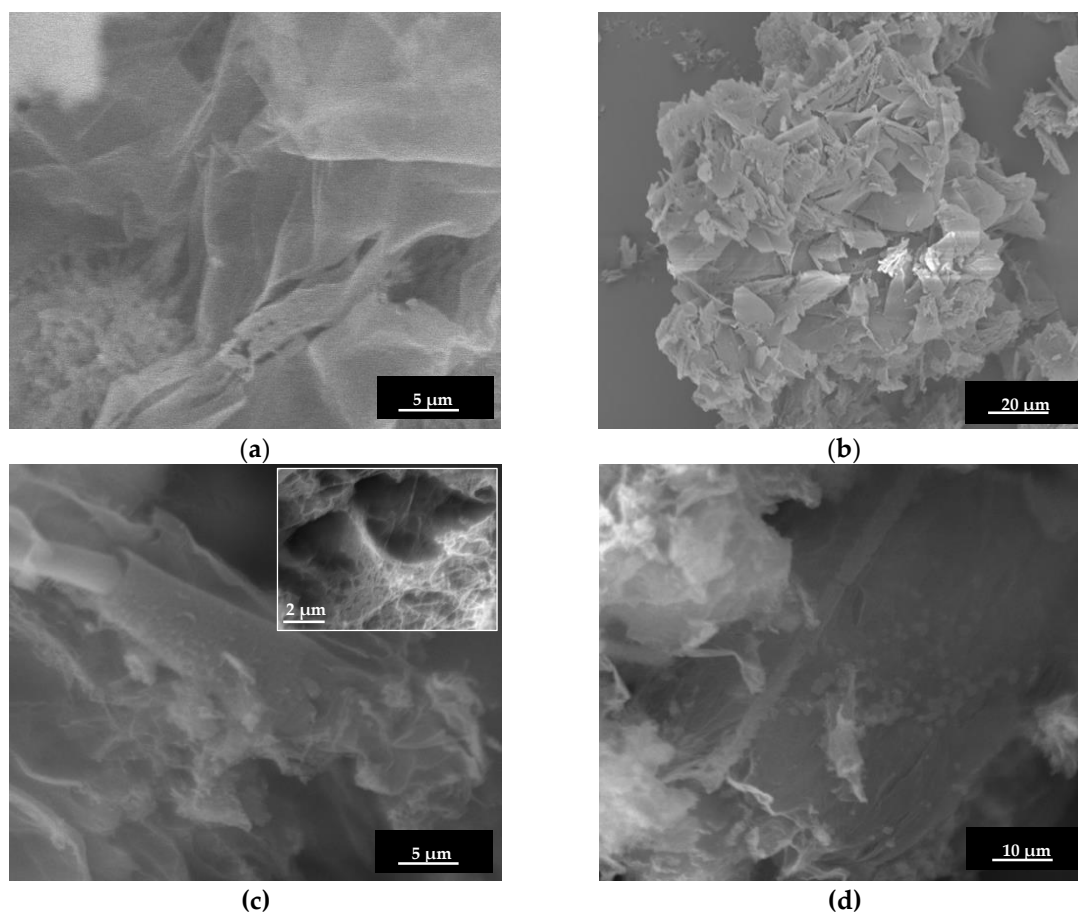
100 spectrometer from 4000 to 400 cm^{-1} using KBr pellets at room temperature. Optical absorption
101 measurement (SHIMADZU UV-1800) was measured. Prior to the measurement, the powder
102 materials were dispersed in water (50 mg of samples in 25 ml water at room temperature). The
103 thermal stability of samples was performed using thermal gravimetric analysis (TGA), Ultra micro
104 balance, Mettler Toledo. An alumina pan was loaded with 5-10 mg of sample material and heated
105 from room temperature to 1273 K at a rate of 10 K/ min in air atmosphere.

106 Nitrogen isotherms were obtained using a porosity analyzer (Micromeritics ASAP2060) at 77 K.
107 The surface areas of the samples were calculated using the Brunauer–Emmett–Teller (BET) method.
108 The total volume of pores was calculated using the software from the BJH adsorption calculation.
109 The CO_2 adsorption and desorption performance were evaluated with a TGA/DSC 3+ micro balance,
110 Mettler Toledo. The CO_2 capture capacity of the sorbents were determined by measuring the mass
111 uptake of the sample during the CO_2 adsorption.

112 3. Results and discussion

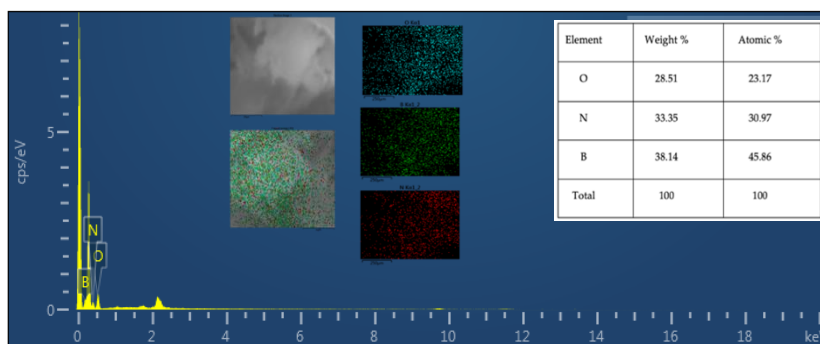
113 3.1. Sample characterisation

114 The morphology of samples was studied using scanning electron microscopy (SEM). The
115 pristine BN exhibited an ultrathin flake-like morphology, as displayed in (Figures 1a–b). BN-P123
116 presented a cloud-like sheet structure with interconnected network of porous structure (Figures 1c–
117 d). Moreover, the formation of pristine BN and BN-P123 were studied by EDX and elemental
118 mapping (Figures 2a–b). It is obvious that the product is mainly comprised of boron (B), nitrogen (N)
119 and oxygen (O). As shown in Figure 2b, BN-P123 has very little increase in oxygen content compared
120 to pristine BN. This is due to the introduction of P123 into BN formation.
121

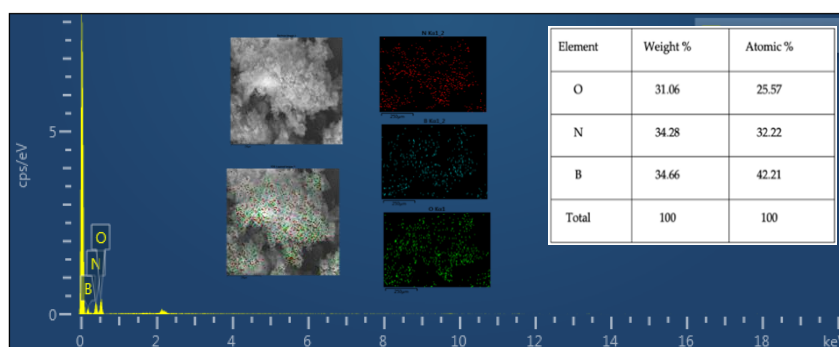


122 **Figure 1.** SEM images of (a, b) pristine BN; (b, c) BN-P123. The insert shows the interconnected porous
123 structure.

124



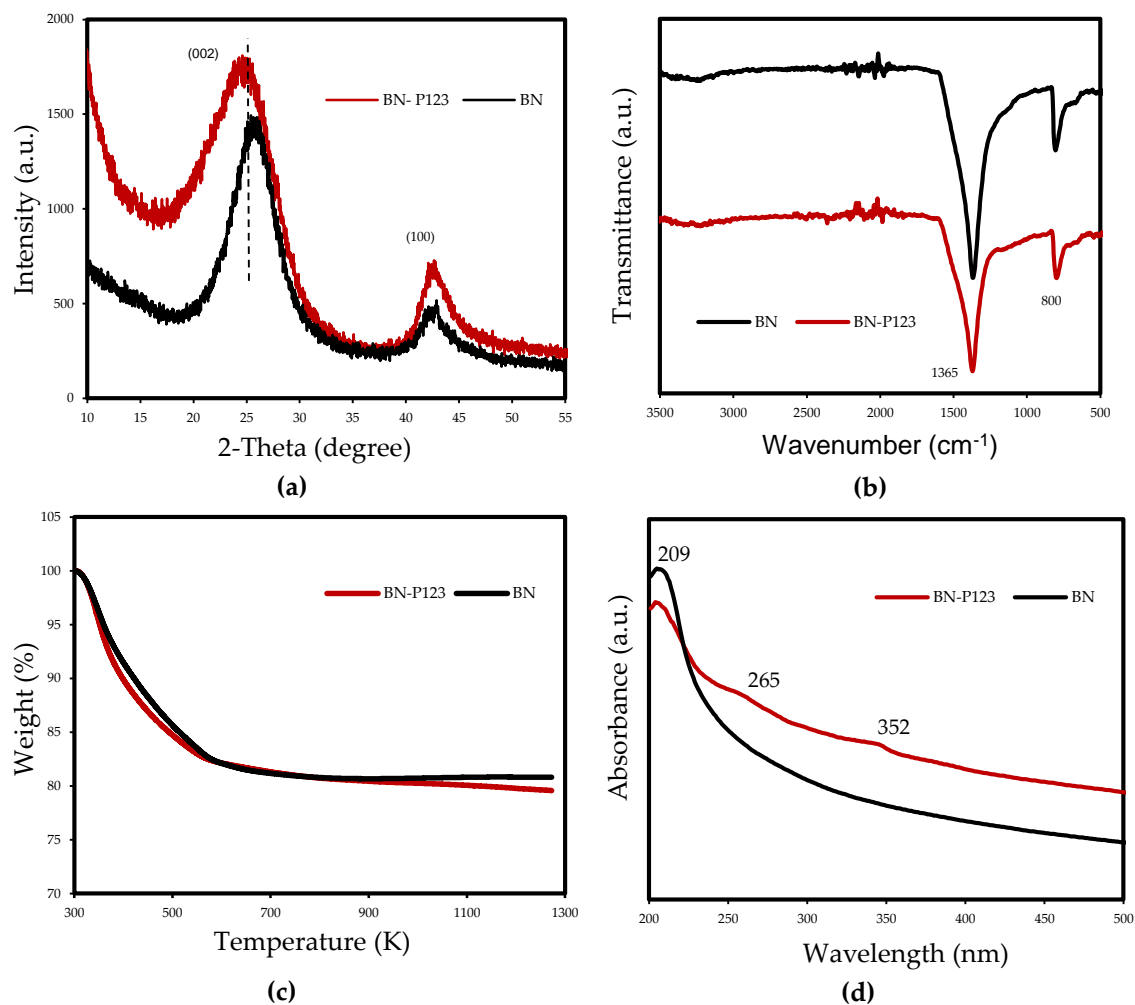
(a)



(b)

125 **Figure 2.** EDX spectra of (a) pristine BN; (b) BN-P123 and the insert show the elemental mapping and
 126 corresponding atomic % of elements.

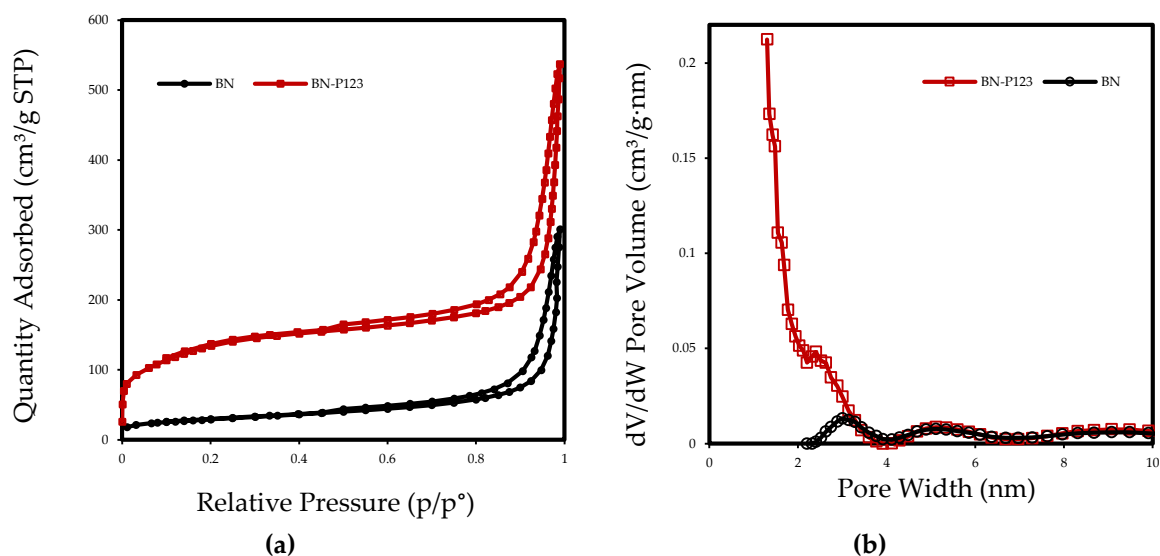
127 The structure of samples was analysed and Figure 3a depicts the XRD patterns of the prepared
 128 samples. The results show two characteristic peaks around $\sim 25^\circ$ and $\sim 42^\circ$ which are attributed to
 129 the (002) and (100) crystal planes of hexagonal boron nitride, respectively [30]. Additionally, the
 130 peaks of both samples confirmed the poor crystallization with the presence of turbostratic material.
 131 Compared with pristine BN, the (002) diffraction peaks of BN-P123 shifted to a lower angle, which
 132 promote more disordered hexagonal boron nitride (h-BN) structure. More details of the chemical
 133 features were supported by Fourier transform infrared (FT-IR) spectroscopy and the results are
 134 shown in Figure 3b. All peaks exhibited two main characteristic bands of boron nitride at ~ 1365 and
 135 800 cm^{-1} corresponding to in-plane B-N transverse optical mode and out-of-plane B-N-B bending
 136 mode, respectively [31]. No major chemical differences could be observed between the samples.
 137 Thermal stability of samples was performed in air atmosphere (rate=10 K/min) and shown in Figure
 138 3c. The TG thermograms reflected the weight loss of 19% for both samples, representing the removal
 139 of moisture adsorbed on the material surface. After 573 K the lines show the thermal stability nature
 140 of BN at high temperature and there was no significant weight loss up to 1273 K. The UV-vis
 141 absorption collected in Figure 3d indicates a highly transparent from visible to UV wavelength [32].
 142 The maximum absorption peak around 209 nm, is attributed to intrinsic excitation absorption band
 143 of h-BN. Besides, small humps around 265 and 352 nm were detected in BN-P123, corresponding to
 144 impurities. So far, above all characteristic results on both samples, it was found that the structure and
 145 chemical nature of BN has not changed after modifying BN with the surfactant compound and both
 146 samples revealed almost similar features. We assumed that the utilisation of block copolymer (P123)
 147 might affect the textural properties of pristine BN.
 148



149 **Figure 3.** XRD patterns (a); FT-IR (b); TGA curves of prepared samples (c) and UV-Vis (d).

150 3.2. Textural Analysis

151 The textural properties of pristine BN and BN-P123 adsorbent were obtained by nitrogen
 152 adsorption/desorption isotherm at 77 K and the results are summarized in Table 1. As indicated in
 153 Figure 4a, the resulting isotherms display a typical type II curve based on IUPAC classification and
 154 type H3 hysteresis loop in the partial pressure range 0.4-1.0, which indicates the presence of mesopores
 155 and slit shape pores [33]. There is a trivial rise in N₂ adsorption-desorption isotherm of BN-P123 at
 156 lower pressure ($P/P_0 < 0.25$), which is caused by presence of micropores [34]. The non-local density
 157 functional theory (NLDFT) was used to calculate pore size distributions. As expected, the dV/dW pore
 158 volume of BN-P123 increases dramatically with abundance of micropores (Figure 4b). Meanwhile,
 159 using the Brunauer–Emmett–Teller (BET) method [35], the specific surface areas are calculated
 160 showing that the BET surface area of BN-P123 is much higher than pristine BN (Table 1). It is clear
 161 from the above measurements that the P123 introduced into precursors during the fabrication process
 162 is highly effective on the microscale structure of porous BN and improves surface area and pore
 163 volume of the sample.



164 **Figure 4.** Nitrogen adsorption-desorption isotherm of the pristine BN and BN-P123 (a); NLDFT pore size
 165 distribution curves of the same samples (b).

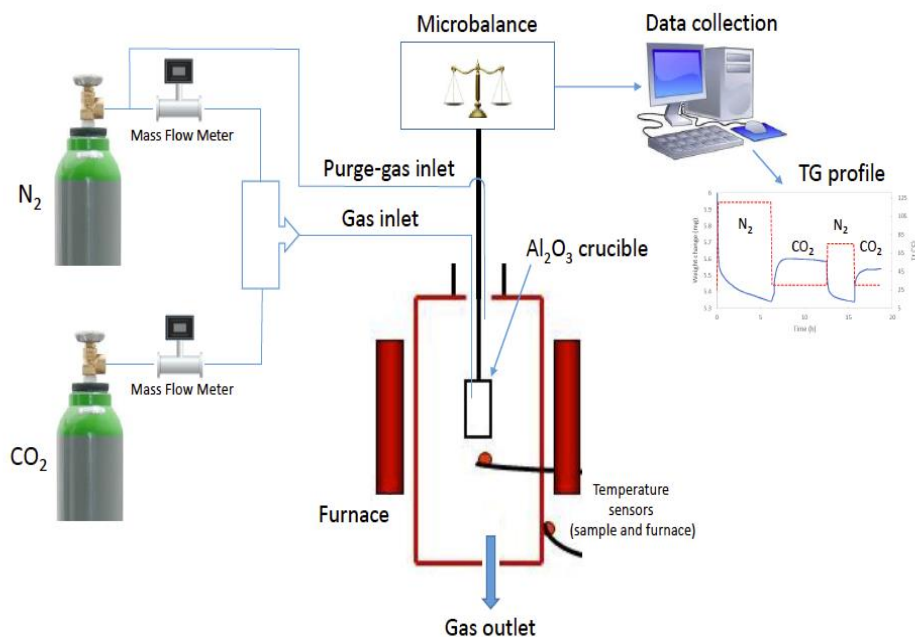
166 Table 1. Textural properties and CO₂ capacity (298 K) of prepared materials.

sample	S_{BET}^1 (m ² /g)	V_{total}^2 (cm ³ /g)	CO ₂ Uptake (mmol/g)
Pristine BN	102	0.46	2.00
BN-P123	476	0.83	2.69

167 ¹ Specific surface area (m²/g) obtained by Brunauer-Emmett-Teller (BET) method. ² Total pore volume (cm³/g)
 168 calculated at $P/P_0 = 0.99$.

169 3.3. Gas adsorption analysis

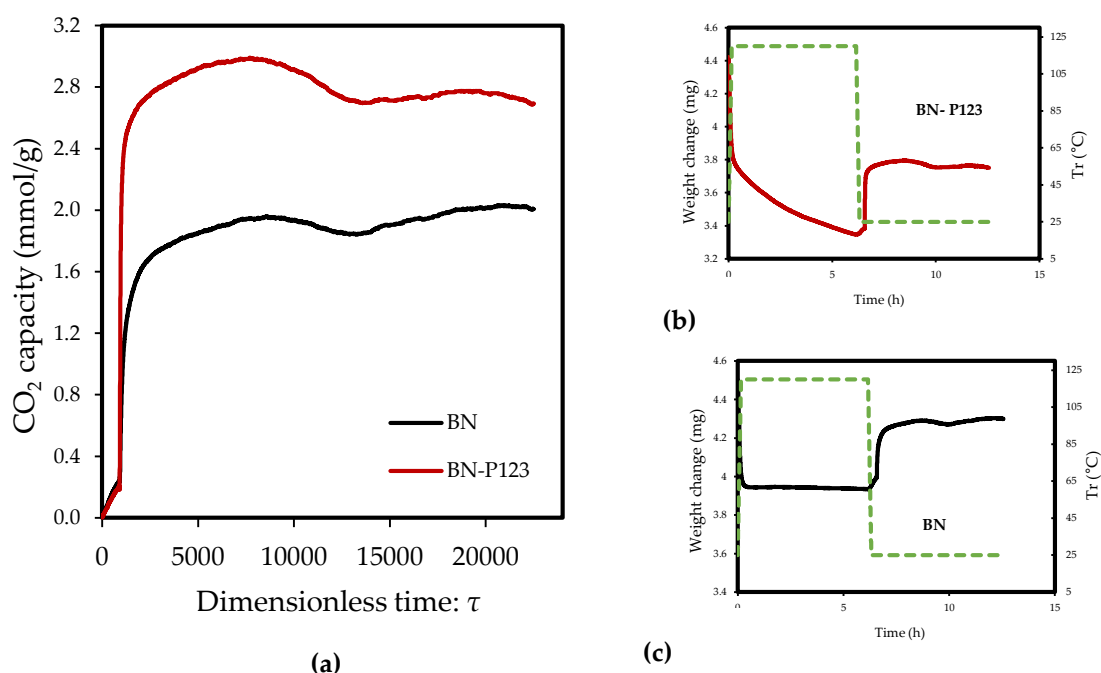
170 Due to the relatively large porosity of samples, the modified sample BN-P123 and pristine BN
 171 were assessed for CO₂ capture under ambient conditions. The adsorption capacities of pure CO₂ on
 172 pristine BN and BN-P123 were determined by thermogravimetric analysis. Prior to the sorption test,
 173 samples were dried at 393 K with a heating rate of 10 K/min from 298 K under flowing N₂ (150
 174 ml/min) for 6 hours and then allowed to cool to the temperature at which the sorption is carried out
 175 at 298 K with a heating rate of 10 K/min. When the sorption temperature was reached, samples were
 176 stabilized under flowing N₂ (99,999%, 150 ml/min) for 15 min and then N₂ flow was switched to pure
 177 CO₂ (99,999%, 50 ml/min) flow for 6 hours. The mass uptake during this stage was interpreted as the
 178 CO₂ capture capacity. Figures 5 and 6 (a-c) illustrate the setup of experiments and the TG profiles of
 179 CO₂ uptake along with weight change results respectively.



180

181

Figure 5. Illustration of CO₂ adsorption experiment.



182

Figure 6. TG profiles of CO₂ adsorption on Pristine BN and BN- P123 (a); TG profiles of weight change on the same samples (b,c).

183

184

185

186

187

188

189

190

191

192

The experiments reveal that pristine BN shows a CO₂ capacity of 2 mmol/g at 298 K, which enhanced with the addition of P123 copolymer (2.69 mmol/g for BN-P123 at 298 K) (Table 1). The augmented CO₂ adsorption on BN-P123 sample is undoubtedly as a result of the porous morphology of modified BN, whereas pristine BN exhibits lower porosity. It is well-known that higher microporosity provides more active sites and storage space to boost the adsorption performances [36,37,38]. To the best of our knowledge, the result of our synthetic method is higher than other modification methods such as (3D) BCNO structure (1.8 mmol/g) at 298 K as reported by Lopez-Salas et al. [39] and closer to porous BCN (2.49 mmol/g) at 298 K and porous BN fiber (2.85 mmol/g) at 273 K [40,41]. However, the use of melamine in porous BCN as well as BN fiber leads to the presence of

193 carbon content and consequently decreases the stability upon exposure to ambient air. The effect of
 194 high-temperature treatment in different gases was studied in [42], where porous BN fibers treated in
 195 NH_3 gas at 1673–1773 K enhanced CO_2 adsorption capacity (from 0.45 mmol/g to 1.6 mmol/g).
 196 Nonetheless, this outcome is not a satisfactory result. One possible insight of this finding is that
 197 pyrolysis temperature and carrier gas does not lead to a remarkable change in CO_2 uptake. In
 198 addition, directing triblock co-polymer was also used to design a hierarchical carbon sorbent [43].
 199 This hierarchical structure is desirable for CO_2 capture as it shows superior capacity (4.5 mmol/g)
 200 under ambient conditions. It is noteworthy that at lower pressures ($\text{bar} \leq 1$), the density of pore
 201 volume, especially the micropores volume plays a critical role in capturing CO_2 [44]. Therefore, high
 202 surface area and porosity of BN-P123 has brought about a positive adsorption interaction.

203 It is to be noted that for the pristine BN (without adding surfactant) the CO_2 adsorption capacity
 204 on our sample exceeds those materials reported by Marchesini et al. [45,46]. Although they
 205 accomplished highly porous boron nitride with a high surface area ($>1900 \text{ m}^2/\text{g}$), the CO_2 adsorption
 206 capacity of their sample was up to 1.6 mmol/g under ambient condition. Given the results of our
 207 approach, one can conclude that though the specific surface area (SSA) is one of the main factors to
 208 increase the CO_2 capacity, obtaining a high SSA e.g. ($>1000 \text{ m}^2/\text{g}$) does not lend itself to an increased
 209 CO_2 capacity.
 210

211 5. Conclusions

212 In summary, the porosity of boron nitride has been successfully tuned by introducing the
 213 triblock copolymer surfactant (P123) during the preparation process of BN precursors. In particular,
 214 we found that by utilizing the P123 into boron and nitrogen precursors leads to improved CO_2
 215 adsorption capacity up to 2.69 mmol/g, as compared with pristine porous BN which was found 2.00
 216 mmol/g. Furthermore, based on the structural properties and morphology results obtained in this
 217 work, we determine that both samples share almost similar chemical features. However, the porosity
 218 of samples revealed a remarkable change and for the sample BN-P123 ($0.83 \text{ cm}^3/\text{g}$), it was virtually
 219 quadrupled as a result of the modification. This significant change is attributed to the formation of
 220 more gases during the decomposition process, thereby creating higher porosity levels. A natural
 221 progression of this work is to describe how textural property parameters of BN lead to higher
 222 interaction between BN and CO_2 molecules. Our work could be extended by exploring other
 223 parameters (e.g. electronic features or surface chemistry of BN), which could influence on BN to
 224 capture more CO_2 . All in all, our analyses demonstrate the applicability of metal-free modification of
 225 BN for enhanced capacity of pure CO_2 .

226 **Funding:** F.H. was partially funded by School of Engineering, London South Bank University.

227 **Acknowledgments:** The Sotacarbo contribution in this work has been carried out within the “Centre of
 228 Excellence on Clean Energy” project (CUP: D83C17000370002), funded by the Regional Government of Sardinia
 229 (FSC 2014-2020).

230 **Conflicts of Interest:** The authors declare no conflict of interest.

231 References

- 232 1. Oschatz, M.; Antonietti, M. A search for selectivity to enable CO_2 capture with porous adsorbents.
 233 *Energy Environ. Sci.* **2018**, *11*, 57–70.
- 234 2. Strielkowski, W.; Lisin, E.; Gryshova, I. Climate policy of the European Union: what to expect from the
 235 Paris agreement. *Rom. J. Eur. Aff.* **2016**, *16*, 68.
- 236 3. Bui, M.; Adjiman, C.S.; Bardow, A.; Anthony, E.J.; Boston, A.; Brown, S.; Fennell, P.S.; Fuss, S.; Galindo,
 237 A.; Hackett, L.A. Carbon capture and storage (CCS): the way forward. *Energy Environ. Sci.* **2018**.
- 238 4. Akinpelumi, K.; Saha, C.; Rochelle, G.T. Piperazine aerosol mitigation for post-combustion carbon
 239 capture. *Int. J. Greenh. Gas Control* **2019**.
- 240 5. Mantripragada, H.C.; Zhai, H.; Rubin, E.S. Boundary Dam or Petra Nova – Which is a better model for

- 241 CCS energy supply? *Int. J. Greenh. Gas Control* **2019**.
- 242 6. Lee, S.-Y.; Park, S.-J. A review on solid adsorbents for carbon dioxide capture. *J. Ind. Eng. Chem.* **2015**, *23*,
243 1–11.
- 244 7. Yang, H.; Xu, Z.; Fan, M.; Gupta, R.; Slimane, R.B.; Bland, A.E.; Wright, I. Progress in carbon dioxide
245 separation and capture: A review. *J. Environ. Sci.* **2008**, *20*, 14–27.
- 246 8. Li, B.; Duan, Y.; Luebke, D.; Morreale, B. Advances in CO₂ capture technology: A patent review. *Appl.*
247 *Energy* **2013**, *102*, 1439–1447.
- 248 9. Férey, G.; Serre, C.; Devic, T.; Maurin, G.; Jobic, H.; Llewellyn, P.L.; De Weireld, G.; Vimont, A.; Daturi,
249 M.; Chang, J.-S. Why hybrid porous solids capture greenhouse gases? *Chem. Soc. Rev.* **2011**, *40*, 550–562.
- 250 10. Wang, J.; Huang, L.; Yang, R.; Zhang, Z.; Wu, J.; Gao, Y.; Wang, Q.; O'Hare, D.; Zhong, Z. Recent
251 advances in solid sorbents for CO₂ capture and new development trends. *Energy Environ. Sci.* **2014**, *7*,
252 3478–3518.
- 253 11. Gargiulo, N.; Pepe, F.; Caputo, D. CO₂ adsorption by functionalized nanoporous materials: a review. *J.*
254 *Nanosci. Nanotechnol.* **2014**, *14*, 1811–1822.
- 255 12. Pardakhti, M.; Jafari, T.; Tobin, Z.; Dutta, B.; Moharreri, E.; Saveh Shemshaki, N.; Suib, S.L.; Srivastava,
256 R. Trends in solid adsorbent materials development for CO₂ capture. *ACS Appl. Mater. Interfaces* **2019**.
- 257 13. Yang, S.; Zhan, L.; Xu, X.; Wang, Y.; Ling, L.; Feng, X. Graphene-based porous silica sheets impregnated
258 with polyethyleneimine for superior CO₂ capture. *Adv. Mater.* **2013**, *25*, 2130–2134.
- 259 14. Mendes, P.A.P.; Ribeiro, A.M.; Gleichmann, K.; Ferreira, A.F.P.; Rodrigues, A.E. Separation of CO₂/N₂
260 on binderless 5A zeolite. *J. CO₂ Util.* **2017**.
- 261 15. Irani, M.; Jacobson, A.T.; Gasem, K.A.M.; Fan, M. Facilely synthesized porous polymer as support of
262 poly(ethyleneimine) for effective CO₂ capture. *Energy* **2018**, *157*, 1–9.
- 263 16. Zhang, J. Design and synthesis of metal organic frameworks for co₂ separation and catalysis 2013.
- 264 17. Cota, I.; Martinez, F.F. Recent advances in the synthesis and applications of metal organic frameworks
265 doped with ionic liquids for CO₂ adsorption. *Coord. Chem. Rev.* **2017**.
- 266 18. Ello, A.S.; de Souza, L.K.C.; Trokourey, A.; Jaroniec, M. Coconut shell-based microporous carbons for
267 CO₂ capture. *Microporous Mesoporous Mater.* **2013**, *180*, 280–283.
- 268 19. Weng, Q.; Wang, X.; Wang, X.; Bando, Y.; Golberg, D. Functionalized hexagonal boron nitride
269 nanomaterials: emerging properties and applications. *Chem. Soc. Rev.* **2016**, *45*, 3989–4012.
- 270 20. Shtansky, D. V.; Firestein, K.L.; Golberg, D. V. Fabrication and application of BN nanoparticles,
271 nanosheets and their nanohybrids. *Nanoscale* **2018**, *10*, 17477–17493.
- 272 21. Sun, Q.; Li, Z.; Searles, D.J.; Chen, Y.; Lu, G.; Du, A. Charge-controlled switchable CO₂ capture on boron
273 nitride nanomaterials. *J. Am. Chem. Soc.* **2013**, *135*, 8246–8253.
- 274 22. Choi, H.; Park, Y.C.; Kim, Y.-H.; Lee, Y.S. Ambient carbon dioxide capture by boron-rich boron nitride
275 nanotube. *J. Am. Chem. Soc.* **2011**, *133*, 2084–2087.
- 276 23. Owuor, P.S.; Park, O.-K.; Woellner, C.F.; Jalilov, A.S.; Susarla, S.; Joyner, J.; Ozden, S.; Duy, L.; Villegas
277 Salvatierra, R.; Vajtai, R. Lightweight hexagonal boron nitride foam for co₂ absorption. *ACS Nano* **2017**,
278 *11*, 8944–8952.
- 279 24. Nag, A.; Raidongia, K.; Hembram, K.P.S.S.; Datta, R.; Waghmare, U. V.; Rao, C.N.R. Graphene analogues
280 of BN: novel synthesis and properties. *ACS Nano* **2010**, *4*, 1539–1544.
- 281 25. Xiao, F.; Chen, Z.; Casillas, G.; Richardson, C.; Li, H.; Huang, Z. Controllable synthesis of few-layered
282 and hierarchically porous boron nitride nanosheets. *Chem. Commun.* **2016**, *52*, 3911–3914.
- 283 26. Chen, Y.; Wang, J.; Chen, Y.; Liu, D.; Huang, S.; Lei, W. One-step template-free synthesis of 3D

- 284 functionalized flower-like boron nitride nanosheets for NH₃ and CO₂ adsorption. *Nanoscale* **2018**.
- 285 27. Chen, S.; Li, P.; Xu, S.; Pan, X.; Fu, Q.; Bao, X. Carbon doping of hexagonal boron nitride porous materials
286 toward CO₂ capture. *J. Mater. Chem. A* **2018**.
- 287 28. Huang, K.; Liang, L.; Chai, S.; Tumuluri, U.; Li, M.; Wu, Z.; Sumpter, B.G.; Dai, S. Aminopolymer
288 functionalization of boron nitride nanosheets for highly efficient capture of carbon dioxide. *J. Mater.*
289 *Chem. A* **2017**, *5*, 16241–16248.
- 290 29. Xiong, J.; Yang, L.; Chao, Y.; Pang, J.; Zhang, M.; Zhu, W.; Li, H. Boron nitride mesoporous nanowires
291 with doped oxygen atoms for the remarkable adsorption desulfurization performance from fuels. *ACS*
292 *Sustain. Chem. Eng.* **2016**.
- 293 30. Kurakevych, O.O.; Solozhenko, V.L. Rhombohedral boron subnitride, B₁₃N₂, by X-ray powder
294 diffraction. *Acta Crystallogr. Sect. C Cryst. Struct. Commun.* **2007**, *63*, i80–i82.
- 295 31. Liu, F.; Yu, J.; Ji, X.; Qian, M. Nanosheet-structured boron nitride spheres with a versatile adsorption
296 capacity for water cleaning. *ACS Appl. Mater. Interfaces* **2015**, *7*, 1824–1832.
- 297 32. Ba, K.; Jiang, W.; Cheng, J.; Bao, J.; Xuan, N.; Sun, Y.; Liu, B.; Xie, A.; Wu, S.; Sun, Z. Chemical and
298 bandgap engineering in monolayer hexagonal boron nitride. *Sci. Rep.* **2017**, *7*, 45584.
- 299 33. Pang, J.; Chao, Y.; Chang, H.; Li, H.; Xiong, J.; Zhang, Q.; Chen, G.; Qian, J.; Zhu, W.; Li, H. Silver
300 nanoparticle-decorated boron nitride with tunable electronic properties for enhancement of adsorption
301 performance. *ACS Sustain. Chem. Eng.* **2018**, *6*, 4948–4957.
- 302 34. Bi, W.; Hu, Y.; Li, W.; Jiang, H.; Li, C. Construction of nanoreactors combining two-dimensional
303 hexagonal boron nitride (h-BN) coating with Pt/Al₂O₃ catalyst toward efficient catalysis for CO
304 oxidation. *Ind. Eng. Chem. Res.* **2018**, *57*, 13353–13361.
- 305 35. Brunauer, S.; Emmett, P.H.; Teller, E. Adsorption of gases in multimolecular layers. *J. Am. Chem. Soc.*
306 **1938**, *60*, 309–319.
- 307 36. Li, J.; Xiao, X.; Xu, X.; Lin, J.; Huang, Y.; Xue, Y.; Jin, P.; Zou, J.; Tang, C. Activated boron nitride as an
308 effective adsorbent for metal ions and organic pollutants. *Sci. Rep.* **2013**, *3*, 3208.
- 309 37. Xiong, J.; Li, H.; Yang, L.; Luo, J.; Chao, Y.; Pang, J.; Zhu, W. Metal-free boron nitride adsorbent for ultra-
310 deep desulfurization. *AIChE J.* **2017**, *63*, 3463–3469.
- 311 38. Liu, F.; Li, S.; Yu, D.; Su, Y.; Shao, N.; Zhang, Z. Template-free synthesis of oxygen-doped bundlelike
312 porous boron nitride for highly efficient removal of heavy metals from wastewater. *ACS Sustain. Chem.*
313 *Eng.* **2018**, *6*, 16011–16020.
- 314 39. López-Salas, N.; Ferrer, M.L.; Gutiérrez, M.C.; Fierro, J.L.G.; Cuadrado-Collados, C.; Gandara-Loe, J.;
315 Silvestre-Albero, J.; del Monte, F. Hydrogen-bond supramolecular hydrogels as efficient precursors in
316 the preparation of freestanding 3D carbonaceous architectures containing BCNO nanocrystals and
317 exhibiting a high CO₂/CH₄ adsorption ratio. *Carbon N. Y.* **2018**, *134*, 470–479.
- 318 40. Florent, M.; Bandosz, T.J. Irreversible water mediated transformation of BCN from a 3D highly porous
319 form to its nonporous hydrolyzed counterpart. *J. Mater. Chem. A* **2018**, *6*, 3510–3521.
- 320 41. Wang, D.; Xue, Y.; Wang, C.; Ji, J.; Zhou, Z.; Tang, C. Improved capture of carbon dioxide and methane
321 via adding micropores within porous boron nitride fibers. *J. Mater. Sci.* **2019**, *54*, 10168–10178.
- 322 42. Liang, J.; Song, Q.; Lin, J.; Huang, Y.; Fang, Y.; Yu, C.; Xue, Y.; Liu, Z.; Tang, C. Pore structure regulation
323 and carbon dioxide adsorption capacity improvement on porous BN fibers: Effects of high-temperature
324 treatments in gaseous ambient. *Chem. Eng. J.* **2019**, *373*, 616–623.
- 325 43. To, J.W.F.; He, J.; Mei, J.; Haghpanah, R.; Chen, Z.; Kurosawa, T.; Chen, S.; Bae, W.-G.; Pan, L.; Tok, J.B.-
326 H. Hierarchical N-doped carbon as CO₂ adsorbent with high CO₂ selectivity from rationally designed

- 327 polypyrrole precursor. *J. Am. Chem. Soc.* **2016**, *138*, 1001–1009.
- 328 44. Li, Y.; Ben, T.; Zhang, B.; Fu, Y.; Qiu, S. Ultrahigh gas storage both at low and high pressures in KOH-
- 329 activated carbonized porous aromatic frameworks. *Sci. Rep.* **2013**, *3*, 2420.
- 330 45. Marchesini, S.; Regoutz, A.; Payne, D.; Petit, C. Tunable porous boron nitride: Investigating its formation
- 331 and its application for gas adsorption. *Microporous Mesoporous Mater.* **2017**, *243*, 154–163.
- 332 46. Marchesini, S.; McGilvery, C.M.; Bailey, J.; Petit, C. Template-free synthesis of highly porous boron
- 333 nitride: insights into pore network design and impact on gas sorption. *ACS Nano* **2017**, *11*, 10003–10011.
- 334



© 2019 by the authors. Submitted for possible open access publication under the terms and conditions of the Creative Commons Attribution (CC BY) license (<http://creativecommons.org/licenses/by/4.0/>).

335